Dynamic contrast-enhanced magnetic resonance imaging at 1.5 Tesla with gadopentetate dimeglumine to assess the angiostatic effects of anginex in mice.

Please check the document version of this publication:

• A submitted manuscript is the version of the article upon submission and before peer-review. There can be important differences between the submitted version and the official published version of record. People interested in the research are advised to contact the author for the final version of the publication, or visit the DOI to the publisher's website.
• The final author version and the galley proof are versions of the publication after peer review.
• The final published version features the final layout of the paper including the volume, issue and page numbers.
Link to publication

Dynamic contrast-enhanced magnetic resonance imaging at 1.5 Tesla with gadopentetate dimeglumine to assess the angiostatic effects of anginex in mice

Q.G. de Lussanet[a,b], R.G.H. Beets-Tan[a], W.H. Backes[a], D.W.J. van der Schaft[c,d], J.M.A. van Engelshoven[a,b], K.H. Mayo[e], A.W. Griffioen[c,d,*]

[a]*Department of Radiology, Maastricht University Hospital, Maastricht, The Netherlands*
[b]*Cardiovascular Research Institute Maastricht (CARIM), Maastricht University, Maastricht, The Netherlands*
[c]*Angiogenesis Laboratory, Department of Internal Medicine and Department of Pathology, Maastricht University Hospital, Maastricht, The Netherlands*
[d]*Research Institute for Growth and Development (GROW), Maastricht University Hospital, Maastricht, The Netherlands*
[e]*Department of Biochemistry, University of Minnesota Health Sciences Center, Minneapolis, MN, USA*

Abstract

The purpose of this study was to evaluate the effects of anginex on tumour angiogenesis assessed by dynamic contrast-enhanced magnetic resonance imaging (DCE-MRI) on a clinical 1.5 Tesla MR system and with the clinically available contrast agent gadopentetate dimeglumine. C57BL/6 mice carrying B16F10 melanomas were treated with anginex, TNP-470 or saline. Tumour growth curves and microvessel density (MVD) were recorded to establish the effects of treatment. DCE-MRI was performed on day 16 after tumour inoculation, and the endothelial transfer coefficients of the microvessel permeability surface-area product (K^{PS}) were calculated using a two-compartment model. Both anginex and TNP-470 resulted in smaller tumour volumes ($P < 0.0001$) and lower MVD ($P < 0.05$) compared to saline. Treatment with anginex resulted in a 64% reduction ($P < 0.01$) of tumour K^{PS} and TNP-470 resulted in a 44% reduction ($P = 0.17$), compared to saline. DCE-MRI with a clinically available, small-molecular contrast agent can therefore be used to evaluate the angiostatic effects of anginex and TNP-470 on tumour angiogenesis.
© 2004 Elsevier Ltd. All rights reserved.

Keywords: Angiogenesis inhibitors; Angiostatic agents; Anginex; B16 melanoma; Gd-DTPA; Gadopentetate dimeglumine; Mice; Microvascular permeability; MRI; MRI, functional; TNP-470

1. Introduction

Angiogenesis is essential to normal bodily processes such as embryogenesis and wound healing, but it is also a key regulator of various pathological disorders, including tumour growth, arthritis, endometriosis, atherosclerosis and diabetic retinopathy [1,2]. The targeting of blood vessels is considered a potentially useful anticancer strategy, primarily because endothelial cells are more accessible than other cells to pharmacological agents delivered via the blood, and because they are genetically stable and thus not easily mutated into drug-resistant variants. Anti-angiogenesis therapy could be a promising modality in the future, either as monotherapy or in combination with conventional cancer therapy [1]. The search for new inhibitors of angiogenesis with reduced toxicity, improved potency, stability, selectivity and ease of delivery is an important field of research. A revolutionary development in this search has been the design of small, cytokine-like peptides that contain only selective domains of traditional anti-angiogenesis agents in order to create well-defined antitumour agents that focus on specific angiogenesis processes. This approach produced anginex, which was designed

---

according to the three-dimensional, β-sheet structure of α-chemokines such as platelet factor 4 and interleukin 8 [3].

In vitro anginex acts by blocking the adhesion and migration of activated endothelial cells [3], leading to cell detachment, a process that is called anoikis, and the subsequent induction of apoptosis. *In vivo* anginex targets angiogenically activated (tumour) endothelial cells and inhibits angiogenesis, ultimately leading to anticancer activity in mice, both as a single therapy and in combination with chemotherapy [4], with no toxic effects observed thus far [5].

Generally accepted standards of reference for evaluating angiogenesis activity and the effects of treatment are the histological assessment of microvessel density (MVD) and the measurement of circulating angiogenesis factors. The reliability of these surrogate markers is subject to considerable dispute. New techniques for monitoring the effects of anti-angiogenesis treatment that are less or non-invasive are currently under investigation [6]. Dynamic contrast-enhanced, T_1-weighted magnetic resonance imaging (DCE-MRI) [6–9] is a non-invasive imaging technique that can be used to derive microcirculation properties that mark tumour angiogenesis [7,10]. Various models have been investigated that relate changes in signal intensity over time as measured with DCE-MRI to tumour activity. The most effective models are those that convert the measured changes in signal intensity into changes in contrast-agent concentration and subsequently apply a pharmacokinetic two-compartment analysis. Two-compartment analysis yields parameters for a plasma fraction (f^{PV}) within the tumour and a rate of exchange between the blood and interstitial compartments (i.e. a transfer coefficient, K^{PS}) [8]. Applications of DCE-MRI in animal MR systems and with experimental, large-molecular contrast agents effectively showed reductions in f^{PV} and K^{PS} in the rim of solid tumours after treatment with anti-angiogenesis agents [8] including the fumagillin derivative TNP-470 [10]. Currently, such large-molecular contrast agents are unsuitable for DCE-MRI in man. Preliminary evidence suggests that DCE-MRI studies are reproducible when using clinical 1.5 Tesla MR systems and clinically approved, small-molecular contrast agents [11,12].

It was hypothesised that the anti-angiogenesis mechanism of anginex will lead to a decreased tumour MVD and to maturation of the vasculature, which would be expected to reduce the tumour transfer coefficient. The aim now was therefore to evaluate the anti-angiogenesis effects of the angiostatic compounds anginex and TNP-470 on tumour angiogenesis assessed by DCE-MRI on a clinical 1.5 Tesla MR system and with the clinically available contrast agent gadopentetate dimeglumine.

2. Materials and methods

2.1. Mouse tumour model

The local ethical review committee approved the animal experiments. B16F10 melanoma cells (provided by Dr J. Fidler, Texas) were cultured in minimal essential medium (MEM) with Hank's salts, 10% fetal calf serum (BioWhittaker, Verviers, Belgium), 50 IU/ml penicillin (ICN, Aurora, Ohio) and 50 IU/ml streptomycin (Seva, Heidelberg, Germany), MEM vitamins, 2-mM L-glutamine, non-essential amino acids and 2 mM sodium pyruvate. Cells were harvested with trypsin (0.125%) (DIFCO, Detroit, Michigan). At day 0, 6-week-old C57BL/6 mice ($n = 34$) (obtained from Charles River, Heidelberg, Germany) were inoculated subcutaneously in the right flank with 2×10^5 B16F10 cells. Once tumours became visible, between day 6 and 9, each one was measured daily with a calliper and tumour volumes were recorded, calculated as width$^2 \times$length$\times 0.52$ [13]. Mice were randomised and treated with anginex ($n = 14$), the established angiogenesis inhibitor TNP-470 ($n = 9$) or saline (0.9% NaCl solution) alone ($n = 11$), using previously optimised drug dosages and modes of administration [3,14]. Anginex [3], dissolved in saline, was administered (6 mg/kg body wt per day) from day 0 through a surgically implanted Alzet osmotic minipump (Durect, Cupertino, CA). TNP-470 (provided by Takeda Chemical Industries, Osaka, Japan), dissolved in saline with 3% ethanol and 5% glucose (just before treatment diluted from a stock of 30 mg/ml in dimethyl sulphoxide), was administered by intraperitoneal injection (60 mg/kg body wt) every other day. Treatment with TNP-470 was started from day 9 to allow the formation of an early-stage tumour and prevent toxic effects due to prolonged treatment.

2.2. MRI

On day 16, 13 mice from the population described above, with volume-matched tumours to exclude tumour size-dependent differences [10], were selected for MRI (saline, $n = 5$; anginex, $n = 5$; TNP-470, $n = 3$). Before imaging the mice were anaesthetised by subcutaneous injection of 100 mg/kg body wt ketamine (Nimatek; Eurovet, Bladel, The Netherlands) and 10 mg/kg xylazine (Sedamun; Eurovet), and the subcutaneous osmotic minipumps were removed. MRI was as previously reported [12], using a circular surface coil (5 cm dia.) and a 1.5 Tesla system (Intera; Philips, Best, The Netherlands). A T_2-weighted acquisition [multislice turbo-spin echo, echo-train length 28, repetition time (TR) 3.3 s, echo time (TE) 200 ms, flip angle (FA) 90°] that covered the tail-end half of the mouse was used for tumour delineation, with 16 transverse sections, a field of view of $44 \times 64 \times 32$ mm (anterior-posterior$\times$left-right$\times$feet-head),

matrix dimensions of 88×128, pixel size 0.5×0.5, and slice thickness 2.0 mm. Six T_1-weighted acquisitions [three-dimensional fast-field echo (3D FFE), TR 50 ms, TE 7 ms] were performed with different FA ($2°$, $5°$, $10°$, $15°$, $25°$ and $35°$) to determine the local T_1-relaxation times before contrast enhancement [15]. Subsequently, a T_1-weighted, dynamic contrast-enhanced series of 50 scans (3D-FFE: TR 50 ms, TE 7 ms, FA $35°$), 39 s/volume acquisition) was conducted, with 16 transverse sections, a field of view of $44 \times 64 \times 32$ mm, matrix dimensions of 88×128, a slice thickness of 4.0 mm, and pixel size 0.5×0.5 mm. Adjacent sampled sections were 2.0 mm displaced and subsequently interpolated to 16 2.0 mm-thick sections during reconstruction. Gadopentetate dimeglumine (Magnevist; Schering AG, Berlin, Germany; 0.1 mmol/kg body wt) was manually infused into the tail vein with 15 µl of saline to 'flush' the injected volume. Administration of the total injection volume was standardised by timing the (slow) injection duration of 30 s to prevent the high concentrations that might cause susceptibility artefacts. Injection of contrast agent was started at the onset of the fifth scan of the dynamic series. The temperature in the magnet bore was maintained at 28 °C.

2.3. Analysis of MRI data

The T_2-weighted anatomical acquisitions were used to locate and delineate the tumour from the surrounding tissue and oedema. A region of interest was manually drawn around the whole tumour volume in the central slice though the tumour. This region of interest was used for further analysis. Regions of interest for the tumour rim were defined as the approximately 1 to 2 mm-thick peripheral zone of strong contrast enhancement [7] in the dynamic T_1-weighted series; the tumour core was the remaining central region.

Kinetic analysis of the images was performed as described previously [12]. Local time-averaged T_1 relaxation rates of the precontrast images (R_{10}) and the postcontrast image (R_1) signal-intensity changes over time (Fig. 1) were used to determine the time course of the plasma concentration in the aorta, representing the arterial input function and tissue concentration in the tumour. Individual input functions were used to correct for small variations in the manual injection of the contrast agent, intrinsic circulation properties and contrast elimination. The plasma $R_1(t)$ time course was fitted to a bi-exponential function. The constant (i.e. T_1 relaxivity) describing the ratio of R_1 change to contrast-agent concentration has been found [12] to be 5.6 mM^{-1} per s by *in vitro* measurements of mouse plasma (with citrate buffer) concentrations at 1.5 Tesla. A pharmacokinetic, two-compartment, bidirectional exchange model [12,16,17] was used to determine the tumour endothelial transfer coefficient (K^{PS}), reflux coefficient (k) and
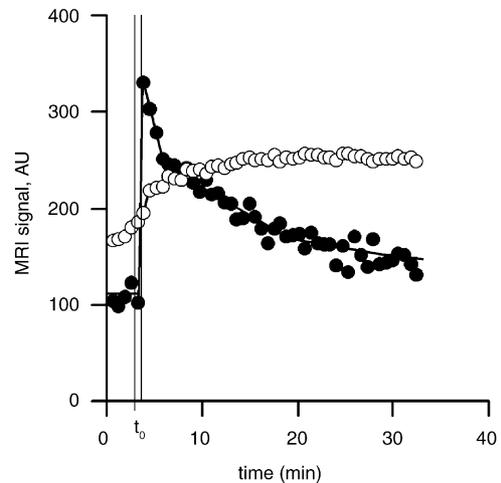

Fig. 1. Dynamic contrast-enhanced magnetic resonance imaging for measuring signal-intensity changes over time in blood and tumour. Signal-intensity (SI, arbitrary units) time courses (●) measured in the aorta show immediate increases after injection (t_0) of the contrast agent gadopentetate dimeglumine, followed by a bi-exponential decline. No recirculation peak is observed, because the duration of contrast-agent injection and dynamic-volume acquisitions were longer than blood circulation times in mice. Average signal-intensity time courses measured in the tumour (○) show more gradual increases than in the blood, which diminish again approximately 15 min after injection (t_0).

fractional plasma volume (f^{PV}) for each voxel. K^{PS} and k were expressed as ml/min per 100 cm^3 of tissue and f^{PV} were expressed as ml/100 cm^3 of tissue. It was previously shown (12) that for this model, using gadopentetate dimeglumine, the K^{PS} is of main interest for indexing angiogenesis activity. Colour-coded K^{PS} maps, overlaid on the corresponding T_1-weighted image (as illustrated in Fig. 2), were used for defining regions of interest for which K^{PS}, f^{PV} and k were spatially averaged for the whole tumour, the tumour rim and the core. The data processing was performed in the *MATLAB* programming environment (The MathWorks, Natick, MA).

2.4. MVD

On day 16, all mice were killed by cervical dislocation under narcosis and tumours were excised. From these tumours, axial cryosections (5 µm) corresponding to the MRI sections were cut and stained immunohistochemically using anti-CD31 antibody (followed by goat anti-rat PO and DAB development). MVD was evaluated as described previously [18]. In brief, two independent observers assessed MVD by counting the number of vessels in three high-power fields randomly selected within a section. In addition, MVD maps were generated for the tumours of mice that underwent DCE-MRI by counting blood vessels in microscopic fields of 0.45×0.45 mm^2 (magnification $250 \times$) for a full tumour section.
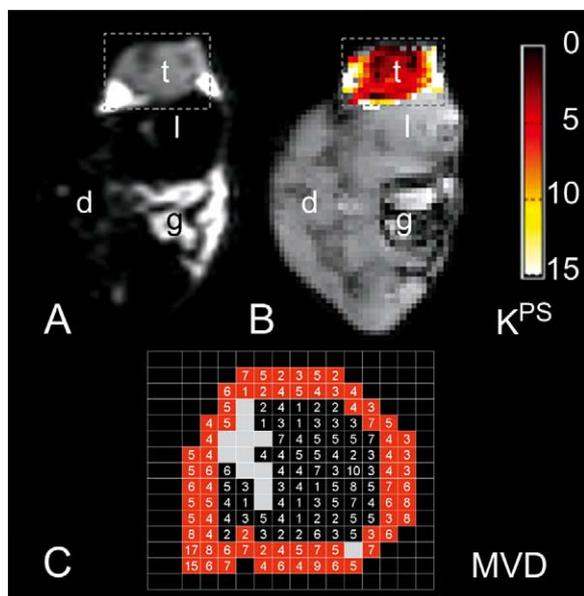
Fig. 2. Transfer coefficient (K^{PS}) and microvessel density (MVD) maps in a control mouse. (A) On the axial T_2-weighted image of the mouse, tumour (t) tissue (grey) and oedema (white) are clearly discernible from adjacent muscle tissue (nearly black) of the hind leg (l), within the grey dotted box; d, dorsal side; g, gut. (B) Maps of K^{PS} (ml/min per 100 cm^3 of tissue), in pseudo-colour (scale on the right) are superimposed on the T_1-weighted image. Areas of low K^{PS} correspond to darker areas in the tumour on the T_2-weighted image and were identified as necrotic regions on histological sections of the tumour in the same axial orientation as the MRI slices. (C) Maps of the MVD (vessels/0.2 mm^2) of the CD-31-stained histological section show a higher mean MVD for the tumour rim (red, MVD = 5.2±2.6 (SD)) compared to the core (black, MVD = 3.8±1.9), as well as necrotic regions (grey fields).

2.5. Statistical analysis

Tumour growth curves for the anginex, TNP-470 and saline treatment groups were compared by two-way analysis of variance. MVD, K^{PS}, k, and f^{PV} for the different treatment groups, and rim and core MVD in the MVD maps, were compared by unpaired, two-sided Student t-tests. Intratumour rim and core K^{PS}, k and f^{PV} were compared for the treatment and control groups by paired, two-sided Student t-tests. K^{PS}, k, and f^{PV} for the different treatment groups were also evaluated using the Mann-Whitney test to account for possible non-normal distribution of variables. Statistical analyses used commercial software (*SPSS 10.0.5*; SPSS Inc., Chicago, IL) and the level of significance was set at $P < 0.05$.

3. Results

3.1. Antitumour activity of TNP-470 and anginex

Anginex inhibited tumour growth by 68% ($P < 0.0001$), as compared to growth in saline control mice (Fig. 3A). TNP-470 showed 65% inhibition ($P < 0.0001$) of tumour growth, as compared to saline control mice (Fig. 3A). Tumour MVD was reduced by approximately 50% for both anginex and TNP-470 ($P < 0.05$; Fig. 3B). Toxic effects were observed after TNP-470 treatment, but not after anginex (data not shown).

3.2. K^{PS} for tumour vessels by MRI in mice treated with anginex

Clear tumour delineation and differentiation from adjacent muscle tissue and oedema was possible with the T_2-weighted acquisition (Fig. 2A). K^{PS} in tumours, calculated using T_1-weighted DCE-MRI measurements, showed a decrease of 64% ($P < 0.01$) in anginex-treated mice as compared with K^{PS} in tumours of saline control mice (Table 1). Reductions in K^{PS} were most statistically significant in the rim of the tumour (66%, $P < 0.003$). The tumour core showed a 67% reduction in K^{PS}, which almost reached statistical significance ($P = 0.05$; Table 1). MRI on tumours in mice treated with TNP-470 showed decreases in K^{PS} in the whole tumour of 44% ($P = 0.17$), in the rim of 43% ($P = 0.16$) and in the core of 43% ($P = 0.16$) (Table 1). No significant differences
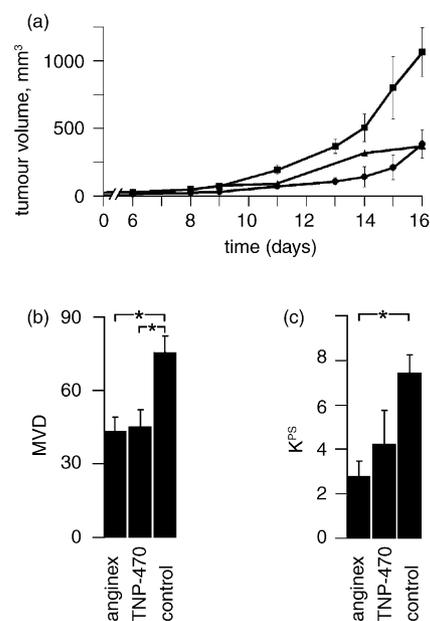
Fig. 3. Inhibition of tumour growth in mice by anginex and TNP-470. (A) Tumour growth curves show significant inhibition for mice treated with anginex (●, started at day 0; $P < 0.0001$) and TNP-470 (▲, started at day 9; $P < 0.0001$) in comparison with saline (■). For clarity, variations in tumour measurements (the SEM was typically 20% in all groups) are only shown for the anginex and the saline groups. (B) Microvessel density (MVD) for tumours of mice treated with anginex, TNP-470 or saline alone (*$P < 0.05$). (C) Transfer coefficient (K^{PS}, ml/min per 100 cm^3 of tissue) values (±SEM) measured in the rim of the tumour, showing similar reductions to those from the MVD measurements (*$P < 0.003$).

Table 1
Dynamic contrast-enhanced magnetic resonance imaging parameters for tumours treated with angiostatic agents

		Saline	Anginex	TNP-470
K^{PS}	Tumour[b]	5.5 ± 0.9[a]	$2.0* \pm 0.4$	3.1 ± 1.2
	Rim[c]	7.4 ± 0.8	$2.8** \pm 0.7$	4.2 ± 1.5
	Core[d]	3.0 ± 0.6	1.3 ± 0.2	1.7 ± 0.5
f^{PV}	Tumour	8.6 ± 3.9	1.9 ± 1.0	7.7 ± 6.7
	Rim	14.4 ± 6.8	2.1 ± 0.5	8.3 ± 7.0
	Core	4.3 ± 2.4	0.9 ± 0.7	5.8 ± 5.2
k	Tumour	10.0 ± 3.4	11.6 ± 4.2	5.5 ± 2.0
	Rim	10.8 ± 3.7	10.1 ± 4.3	6.5 ± 2.9
	Core	7.8 ± 2.7	13.7 ± 5.4	6.8 ± 2.1

K^{PS}, microvessel permeability surface area product (ml/min per 100 cm^{-3} of tissue); f^{PV}, plasma fraction (%); k, reflux rate (ml/min per 100 cm^{-3} of tissue). $*P < 0.01$; $**P < 0.003$.
   [a] Values given are means $\pm$ SEM.
   [b] Measured in the entire slice of the tumour.
   [c] Rim is defined as the outer 50% of the tumour slice.
   [d] Core is defined as the inner 50% of the tumour slice.

($P > 0.5$) were observed between the K^{PS} of mice treated with anginex or TNP-470.

For the tumours in mice that were selected for DCE-MRI, MVD measurements were performed for the full area of the axial cryosections through the centre of the tumour in correspondence to the MRI sections. MVD maps (Fig. 2C) were aligned and compared with their respective K^{PS} maps shown in pseudo-colour (Fig. 2B). A close similarity was observed between MVD and K^{PS} for individual tumours, of which an example from a saline control mouse is presented in Fig. 2. In addition, MVD maps of the saline control tumours show higher values in the rim of the tumour (36% higher, $P < 0.002$) than in the tumour core. This difference was only statistically significant in saline control mice; in anginex-treated mice the difference was non-significantly ($P = 0.3$) reduced by 11%. This finding was in line with the observed K^{PS}, with a stronger rim versus core difference ($P < 0.003$) in saline control mice than in anginex-treated mice ($P = 0.09$) (Table 1).

MRI-based f^{PV} measurements suggested a decrease of plasma fractions, particularly for the tumour rim, in treated mice as compared to saline control mice (Table 1). No significant differences in f^{PV} were observed between the saline control mice and mice treated with anginex ($P = 0.15$) or TNP-470 ($P = 0.3$). Rim vs. core differences in f^{PV}, although not statistically significant, were slightly stronger in saline control mice ($P > 0.1$) than in anginex-treated mice ($P > 0.3$) (Table 1).

MRI-based measurements of the reflux coefficients (k) revealed no significant differences between saline control mice and mice treated with anginex ($P > 0.9$) or TNP-470 ($P > 0.5$) (Table 1). Also, no particular trends were observed in differences between rim and core k for

saline control ($P > 0.08$) mice, anginex- ($P > 0.5$) or TNP-470- ($P > 0.7$) treated mice.

4. Discussion

The results of this study demonstrate that effects of the angiostatic compounds anginex and TNP-470 on tumour angiogenesis can be assessed by DCE-MRI on a clinical 1.5 Tesla MR system and with the clinically available contrast agent gadopentetate dimeglumine. The novel cytokine-like peptide anginex and the established angiogenesis inhibitor TNP-470 were used to treat cancer in a mouse solid tumour model. TNP-470 is a validated angiogenesis inhibitor and was used here as a positive control according to a previously optimised treatment regimen [14]. Both anginex and TNP-470 are examples of angiogenesis inhibition through direct action on endothelial cells, which has been shown as yet to be the most effective strategy for angiogenesis inhibition as a treatment for cancer [1,4].

In animal studies, the angiostatic effects of compounds are generally assessed by measuring MVD or by detecting circulating angiogenesis factors. MVD is a controversial measure for prognosis because (i) it is a non-physiological variable that cannot differentiate functional from non-functional and non-perfused blood vessels, and (ii) it is subject to considerable (inter- and intra-observer) variation. The latter variability made an international methodological consensus for the assessment of MVD necessary [19]. The detection of circulating angiogenesis factors may similarly suffer from excessive variations, but its major limitation is that it is not yet known what responses (increases or decreases) to expect from specific inhibitors. These considerations necessitate the search for other, preferably non-invasive, surrogate markers. Therefore, great attention is directed toward the development of functional imaging techniques, such as positron-emission tomography, computed tomography, MRI and other non-invasive imaging methods [6], which may localise sites of angiogenesis and offer functional data in animal angiogenesis models and in man. The successful use of MRI has been demonstrated in this study.

More importantly, a clinical MR system and a widely available, clinical small-molecular MR contrast agent proved to be applicable for monitoring the effects of anti-angiogenesis agents and to differentiate the amount of angiogenesis activity within a tumour. Our finding of reduced transfer coefficients after treatment with TNP-470, measured at 1.5 Tesla and with a small-molecular contrast agent, is in line with earlier reported [10] reductions in vascularity and permeability measured in another mouse tumour model with a dedicated, high-field, animal MR system and a large-molecular, experimental contrast agent.

It is important to consider the molecular size of the contrast agent used. First, small- and large-molecular contrast agents may differ greatly in their respective blood concentration changes over time, which may have implications for the required acquisition times and the speed of contrast-agent injection in the dynamic contrast-enhanced series. Blood concentration changes can be expected to be rather larger for small-molecular clinical contrast agents, such as gadopentetate dimeglumine, which are rapidly cleared from the circulation, than for large-molecular experimental contrast agents, which have relatively slow clearance rates. To date, however, no large-molecular contrast agent that is suitable for DCE-MRI has reached approval for clinical use. Good but not perfect correlations were shown between MVD and K^{PS} using the gadopentetate dimeglumine contrast agent in a mouse solid tumour model [12]. Based on that study, as well as the results of our dynamic contrast-enhanced measurements (Fig. 1), we assume our temporal resolution to be sufficient for deriving reliable K^{PS}. As is shown in Fig. 1, with a temporal scan resolution of 39 s and a relatively slow speed of injection, sufficient samples were obtained in the rising part of the tissue signal-intensity curve and the declining part of the vascular-input function.

A second reason for regarding the molecular size of the contrast agent used is to explore which physiological properties are reflected by the K^{PS}. For small-molecular contrast agents the K^{PS} represents the permeability surface-area product (PS) that is to some extent contaminated by flow, as has been shown in a rat tumour model [20]. Both permeability and flow are suitable microcirculatory properties for characterising the status of tumour vascularisation and are likely to decrease during vascular normalisation. Reductions in K^{PS} after treatment with anginex and TNP-470, which were well correlated with reductions in MVD, could have resulted from reduced microvessel permeability, reduced microvessel surface area (per volume of tissue), reduced blood flow, or a combination of these [8]. A study [21] using a rat breast cancer model showed significant reductions in K^{PS} with the use of large-molecular contrast agents after anti-angiogenesis treatment with anti-vascular endothelial growth factor (VEGF) antibody, but failed to measure these reductions in K^{PS} with the use of small-molecular contrast agents. The anti-angiogenesis effects of anti-VEGF antibody primarily target the initiation of angiogenesis, which involves the induction of microvessel permeability by VEGF [1,2], whereas TNP-470 and anginex directly target endothelial cells involved in new vessel formation [1–5,14]. Therefore, the success of using small-molecular agents to measure the effects of anti-angiogenesis treatment might depend on their biological effects. Other reasons might lie in the details of the applied MRI protocol. For example, we feel that, to monitor the concentration changes, a low

rate of contrast-agent injection, rather than high-speed bolus injection (as used in other studies [21]), is essential for rapidly diffusing, small contrast-agent molecules.

The finding that anti-angiogenesis compounds eliminated the rim-core difference in K^{PS} supports the suggestion that treatment with angiostatic compounds can normalise the angiogenesis phenotype of the tumour blood vessels, since angiogenesis is generally most prominent in the rim of a tumour [1,2].

Variations in f^{PV} were too great to reflect significant reductions in blood volume, which may have resulted from the fast diffusion properties of the small-molecular contrast agent. The diagnostic value of the f^{PV} might be better with the future development of large-molecular contrast agents that are safe for injection in man.

The diagnostic value of the reflux parameter (k), derived from the two-compartment model, needs further assessment. Reflux k is commonly set to zero in DCE-MRI studies that use large- molecular contrast agents [7,16]. In our study, k was calculated, but no conclusions were drawn that pertained to differences between treatment groups or differences within a tumour.

Technological advances might optimise DCE-MRI: for example, the development of dedicated MR receiver coils [11] that facilitate faster temporal resolutions and/or increase image quality to further improve K^{PS} and f^{PV} measurements. The rationale for seeking further to improve DCE-MRI using clinical MR systems and clinical contrast agents is ultimately to create a functional imaging tool that may be used in standard oncological MRI protocols. DCE-MRI could be of additional value because its functional parameters might objectify the effects of anti-angiogenesis treatment, possibly even before longer time-scale morphological changes, such as reduction in tumour size, become apparent. DCE-MRI might prove a valuable tool for tumour detection, delineation and staging, as well as for differentiating active regions from non-active or necrotic regions within a tumour, and for the optimisation of individual anti-tumour treatments. Advances in the areas of MRI contrast agents, pharmacokinetic models, imaging techniques and MRI systems, as well as developments in cancer treatments, are continuing. Our preliminary results suggest that DCE-MRI with a clinical 1.5 Tesla MR system and a widely available, small-molecular contrast agent may be used to evaluate the effects of angiostatic compounds on tumour angiogenesis in an animal solid tumour model.

A limitation of this study is that the measured inhibition of tumour angiogenesis using DCE-MRI in this melanoma tumour mouse model after treatment with anginex and TNP-470 may not predict the effects of other anti-cancer treatments in different tumour models. Nor do our results predict K^{PS} or f^{PV} after treating human tumours with either anginex or TNP-470. Further work will be needed using optimised protocols for

human participants to evaluate whether DCE-MRI can indeed successfully demonstrate the effects of anti-angiogenesis treatment in patients with solid tumours.

Acknowledgements

References

1. Griffioen AW, Molema G. Angiogenesis: potentials for pharmacologic intervention in the treatment of cancer, cardiovascular diseases, and chronic inflammation. *Pharmacol Rev* 2000, **52**, 237–268.

2. Folkman J. Angiogenesis in cancer, vascular, rheumatoid and other disease. *Nat Med* 1995, **1**, 27–31.

3. Griffioen AW, van der Schaft DW, Barendsz-Janson AF, *et al.* Anginex, a designed peptide that inhibits angiogenesis. *Biochem J* 2001, **354**, 233–242.

4. Dings RP, Yokoyama Y, Ramakrishnan S, *et al.* The designed angiostatic peptide anginex synergistically improves chemotherapy and antiangiogenesis therapy with angiostatin. *Cancer Res* 2003, **63**, 382–385.

5. van der Schaft DW, Dings RP, de Lussanet QG, *et al.* The designer anti-angiogenic peptide anginex targets tumor endothelial cells and inhibits tumor growth in animal models. *Faseb J* 2002, **16**, 1991–1993.

6. McDonald DM, Choyke PL. Imaging of angiogenesis: from microscope to clinic. *Nat Med* 2003, **9**, 713–725.

7. Turetschek K, Huber S, Floyd E, *et al.* MR imaging characterization of microvessels in experimental breast tumors by using a particulate contrast agent with histopathologic correlation. *Radiology* 2001, **218**, 562–569.

8. Padhani AR. Dynamic contrast-enhanced MRI in clinical oncology: current status and future directions. *J Magn Reson Imaging* 2002, **16**, 407–422.

9. Choyke PL, Dwyer AJ, Knopp MV. Functional tumor imaging with dynamic contrast-enhanced magnetic resonance imaging. *J Magn Reson Imaging* 2003, **17**, 509–520.

10. Bhujwalla ZM, Artemov D, Natarajan K, *et al.* Reduction of vascular and permeable regions in solid tumors detected by macromolecular contrast magnetic resonance imaging after treatment with antiangiogenic agent TNP-470. *Clin Cancer Res* 2003, **9**, 355–362.

11. Kiessling F, Heilmann M, Vosseler S, *et al.* Dynamic T1-weighted monitoring of vascularization in human carcinoma heterotransplants by magnetic resonance imaging. *Int J Cancer* 2003, **104**, 113–120.

12. de Lussanet QG, Backes WH, Griffioen AW, *et al.* Gadopentetate dimeglumine versus ultrasmall superparamagnetic iron oxide for dynamic contrast-enhanced MR imaging of tumor angiogenesis in human colon carcinoma in mice. *Radiology* 2003, **229**, 429–438.

13. Yokoyama Y, Dhanabal M, Griffioen AW, *et al.* Synergy between angiostatin and endostatin: inhibition of ovarian cancer growth. *Cancer Res* 2000, **60**, 2190–2196.

14. Yamaoka M, Yamamoto T, Ikeyama S, *et al.* Angiogenesis inhibitor TNP-470 (AGM-1470) potently inhibits the tumor growth of hormone-independent human breast and prostate carcinoma cell lines. *Cancer Res* 1993, **53**, 5233–5236.

15. Haacke M, Brown RW, Thompson MR, Venkatesan R. T1 estimation from SSI measurements at multiple flip angles. In Venkatesan R, ed. *Magnetic resonance imaging: physical principles and sequence design,* 1 ed. New York, NY, John Wiley & Sons, Inc, 1999, 654–661.

16. Daldrup H, Shames DM, Wendland M, *et al.* Correlation of dynamic contrast-enhanced MR imaging with histologic tumor grade: comparison of macromolecular and small-molecular contrast media. *Am J Roentgenol* 1998, **171**, 941–949.

17. Tofts PS, Kermode AG. Measurement of the blood-brain barrier permeability and leakage space using dynamic MR imaging. 1. Fundamental concepts. *Magn Reson Med* 1991, **17**, 357–367.

18. Hillen HF, Hak LE, Joosten-Achjanie SR, Arends JW. Microvessel density in unknown primary tumors. *Int J Cancer* 1997, **74**, 81–85.

19. Vermeulen PB, Gasparini G, Fox SB, *et al.* Second international consensus on the methodology and criteria of evaluation of angiogenesis quantification in solid human tumours. *Eur J Cancer* 2002, **38**, 1564–1579.

20. Daldrup HE, Shames DM, Husseini W, *et al.* Quantification of the extraction fraction for gadopentetate across breast cancer capillaries. *Magn Reson Med* 1998, **40**, 537–543.

21. Roberts TP, Turetschek K, Preda A, *et al.* Tumor microvascular changes to anti-angiogenic treatment assessed by MR contrast media of different molecular weights. *Acad Radiol* 2002, **9**(Suppl. 2), S511–S513.